An Accelerated Life Testing Data set for Lithium-Ion Batteries with Constant and Variable Loading Conditions

Kajetan Fricke[1], and Renato G. Nascimento[2], and Matteo Corbetta[3], and Chetan S. Kulkarni[4], and Felipe A. C. Viana[5]

[1,2,5] *Department of Mechanical and Aerospace Engineering, University of Central Florida, Orlando, FL, 32816, USA*
kajetan.fricke@ucf.edu
renato.gn@knights.ucf.edu
viana@ucf.edu
[3,4] *KBR, Inc., NASA Ames Research Center, Moffett Field 94035 CA, USA*
matteo.corbetta@nasa.gov
chetan.s.kulkarni@nasa.gov

ABSTRACT

The development of new modes of transportation, such as electric vertical takeoff and landing (eVTOL) aircraft and the use of drones for package and medical delivery, has increased the demand for reliable and powerful electric batteries. The most common batteries in electric-powered vehicles use Lithium-ion (Li-ion). Because of their long cycle life, they are the preferred choice for battery packs deployed over a lifespan of many years. Thus, battery aging needs to be well understood to achieve safe and reliable operation, and life cycle experiments are a crucial tool to characterize the effect of degradation and failure. With the importance of battery durability in mind, we present an accelerated Li-ion battery life cycle data set, focused on a large range of load levels, for batteries composed of two 18650 cells. We tested 26 battery packs grouped by: (i) constant or random loading conditions, (ii) loading levels, and (iii) number of load level changes. Furthermore, we conducted load cycling on second-life batteries, where surviving cells from previously-aged packs were assembled to second-life packs. The goal is to provide the PHM community with an additional data set characterized by unique features. The aggressive load profiles create large temperature increases within the cells. Temperature effects becomes therefore important for prognosis. Some samples are subject to changes in amplitude and number of load levels, thus approaching the level of variability encountered in real operations. Reassembling of survival cells into new packs created additional data that can be used to evaluate the performance of recommissioned batteries. The data set can be leveraged to develop and test models for state-of-charge and state-of-health prognosis. This paper serves as a companion to the data set. It outlines the design of experiment, shows some exemplifying time-series voltage curves and aging data, describes the testbed design and capabilities, and also provides information about the outliers detected thus far. The data set is publicly available for download on the NASA Ames Prognostics Center of Excellence Data Repository[1].

https://doi.org/10.36001/IJPHM.2023.v14i2.3587

1. INTRODUCTION

The transformation of the transportation sector to environmentally friendlier means observed in recent years is expected to continue in accelerated fashion within the foreseeable future. These sustainable transportation modalities include electric powered cars, electrical vertical take-off and landing aircraft, as well as small fixed-wing aircraft and rotorcraft (drones). What all these vehicle types have in common is that the drivetrain represents the main cost driver, where the battery pack alone can share up to 40% of the overall vehicle cost (Lutsey & Nicholas, 2019). Knowledge about usage based battery degradation is important to ensure cost-optimized, reliable and safe operations. Although recent developments concerning battery types like Lithium-Air (Girishkumar, McCloskey, Luntz, Swanson, & Wilcke, 2010) or Sodium-ion (Hwang, Myung, & Sun, 2017), (Yabuuchi, Kubota, Dahbi, & Komaba, 2014) are promising and might lead to future deployment in electric vehicles, the vast majority of today's electric-powered vehicles relies on packs composed of Lithium-Ion (Li-ion) or Lithium-Polymer (Li-Po) cells.

One crucial component in understanding usage-based battery degradation is the acquisition of large and diverse experimental data sets that can be used for both validation of existing battery degradation models and building new experimental data-based as well as hybrid models. Many battery degrada-

[1] https://www.nasa.gov/intelligent-systems-division/discovery-and-systems-health/pcoe/pcoe-data-set-repository/

tion models rely on electrochemistry-based principles, which can accurately predict the state-of-charge (SOC) and state-of-health (SOH), through carefully performed parameter estimation (Karthikeyan, Sikha, & White, 2008). This parameter estimation process usually requires validation using experimental data. Other battery capacity degradation and remaining useful performance studies that utilize large amounts of experimentally gathered data includes the contribution of (Xing, Ma, Tsui, & Pecht, 2013), where an ensemble model with fused empirical and polynomial regression components was validated against experimental battery capacity data. Purely data-driven approaches and combined electrochemistry and data-based models require a large amount of experimental data for model training and parameter identification (Li, He, Su, & Zhao, 2020) (Shen, Sadoughi, Li, Wang, & Hu, 2020).

While, in literature, various experimental battery life cycle studies are publicly available, gaps still remain. Many available Li-ion battery life cycle studies have been conducted using single battery cells cycled at low current levels, which only partially reflect the cycle behavior of batteries deployed in real applications. Data sets where samples are subject a wide range of different load levels are rarely available. So are data sets with overloading conditions that exceed the cell temperature limits and fully exhaust the cell current limits. Battery life cycle data gathered from aging entire packs as opposed to single cells are only published to a limited extend. On the other hand, such data offers crucial information about batteries stressed at their limits, which is likely to occur in real-life applications.

The data set we present here is characterized by unique features with respect to existing, older data sets, as discussed in the next Section. To achieve this goal, we opted to develop our own testbed, which allowed us to control every aspect of the experimental campaign.

With this approach, we ensured to collect a data set covering a wide range of possible deployments and a balanced design of experiments. The data set is pubicly available and can be downloaded from the NASA Prognostics Center of Excellent Data Repository (*upon acceptance, the link to the data set will be added here.*).

The remainder of this paper is organized as follows. Section 2 offers a brief overview of older experimental studies and how the proposed data set compares against them. Section 3 details the design of experiments. It describes the type of batteries we utilized, the rationale behind the loading profile choice and the recommissioning when only one of the cells failed. Section 4 summarizes the critical features of the data set and shows sample curves, how aging effect was tracked, as well as outliers we detected. Section 5 presents the design of the self-developed test-bed including hardware design and architecture. The paper also describes the repository structure in Section A.

2. LITERATURE REVIEW

This section provides an overview of previously conducted Li-ion battery testing studies, where we want to highlight key findings from each study, possible applications and put them in context of our own work. All data sets listed in the following summary are publicly available.

The Center for Advanced Life Cycle Engineering (CALCE) at the University of Maryland provides a life cycle data set for 15 prismatic CS2 cells. This study focused on different discharge profiles while the charging profiles remain consistent across the entire fleet of batteries. The batteries were divided in 6 groups subjected to different discharge profiles, where constant current discharge levels and variable current levels were used to age the batteries until reaching a defined end of performance capacity level. The different aging characteristics for each group of batteries also comprised partial charge and discharge profiles to simulate life cycle behavior of batteries used in real world applications. In another, similar study, a different prismatic cell type was cycled where, apart from different cycling profiles, also variations in ambient air temperature were applied to some of the battery cell groups. The life cycle studies conducted by CALCE provide an extensive data set for single Li-ion batteries cells taking into account variations in operation environments as as well as realistic user operation characteristics. Publications utilizing the aforementioned data sets include (He, Williard, Osterman, & Pecht, 2011) and (Williard, He, Osterman, & Pecht, 2013).

Sandia National Laboratories conducted a battery life cycle study involving 18650 battery cells of three different chemistry types (NCA, NMC, LFP) under various cycling conditions (Preger et al., 2020). The batteries were cycled on a multi-channel battery testing system placed within a thermal chamber to control ambient air temperature. Different groups of batteries were cycled at different ambient air temperatures, discharge current levels and depth of discharges. Each battery was cycled until reaching 80% of initial capacity which authors defined as EOL for that study. In a further life cycle study Li-ion cells were subjected to cell abuse testing conditions. Here, 18650 cells of four different cell chemistries (LCO, LFP, NCA, NMC) were subjected to increasing current levels at different ambient air temperatures until aborting the cycling procedure when reaching the maximum cell temperature specified by the manufacturer.

Stanford University, in collaboration with MIT, published two battery life cycle data sets using 18650 LFP cells, (Severson et al., 2019; Attia et al., 2020). Both data sets focused mainly on the effect of different charging profiles on capacity degradation, where a large number of different fast charging profiles were applied, while the same discharge profile was used across the entire battery fleet. In the first data set, 135 cells were cycled to EOL and in the second data set further 135 cells until reaching 20% capacity degradation. Both data sets can

be used for battery SOH and remaining useful life (RUL) prediction models, as well as for optimization of charging profiles to minimize battery degradation as function of charging conditions.

The Prognostics Center of Excellence (PCoE) at NASA Ames published four data sets which can be divided into two groups. Two of them provide life cycling data of 18650 battery cells conducted on a testbed in laboratory conditions. In the first study, 34 cells with 2Ah capacity were cycled at discharge current levels up to 4A divided in groups subjected to different loading conditions, ambient temperatures and end-of-discharge (EOD) voltages, until reaching a defined end-of-life (EOL) at 12%, 20% or 30% of capacity degradation (Saha & Goebel, 2007). In a second life cycle study 28 LCO battery cells were cycled at variable loading conditions between 0.5A and 4A (Random walk discharge) or applying pulsed current, where discharge cycles with pauses between sections of applied loading were conducted (Bole, Kulkarni, & Daigle, 2014). The cells were divided into groups cycled at room temperature and controlled ambient air temperature at 40C. Both of the aforementioned data sets collected single-cell data, opposed to entire battery packs. The applied current levels remained in the range of 4A, which, in case of the 2.0Ah and 2.1Ah rated cells used, corresponds to 2 C. Both data sets were used in several studies aiming to forecast SOH and SOC for Li-ion battery cells, where the data was either used for validation of existing models or training of data-based models.

The University of Oxford published a Li-ion battery degradation data set that aims to capture the path-dependence of battery aging (Raj, Wang, Monroe, & Howey, 2020; Raj, 2020). Here, the correlation of both aging modes, calendar aging at rest and cyclic aging is considered while aging profiles are applied to 4 groups of cells. Two groups are aged according to one day of cycling and 5 days of aging at rest, and the other two groups are aged at two days of cycling and ten days of aging at rest. The study gives insights about degradation mechanisms that depend on both aging modes.

The‘‘Electric Vehicle Enhanced Range, Lifetime and Safety Through Ingenious Battery Management’’ project published a data set that focuses on capacity loss as function of different ambient air temperature ad life cycling at different C-rates. This data set contains a total of 28 Li-ion cells type 18650 subject to different ambient air temperatures as well as charge and discharge rates. The intent was to gathered data on different environmental conditions that can be encountered during real-world electric vehicle operations (Trad, 2020; Govindarajan, 2021; Trad, 2021).

2.1. Novelty of the Proposed Data Set

Differently from existing works, the data we present in this manuscript addresses aging of pack-level specimens, including electrode connection and wiring, rather than studying degradation of single cells. We aged the battery packs at a wide range of current levels, up to 8 C, hitting the maximum current rating suggested by the manufacturer. On the other hand, most data sets we found focused on discharge current levels in the 1 C - 3 C range. This unique property allows the study of batteries under realistic loading profiles. Some of the samples (i.e, some of the batteries) are subject to a single load level throughout their life, some are subject to two load levels, and some are subject to three load levels. This create a unique variety of aging profiles. The high current profiles enable the recording of the temperature build-up as a direct effect of power dissipation during discharge, which is an important variable to develop prognostic models. Contrarily, existing studies focus on different ambient air temperatures. Additionally, this data set extends the life cycle study to recommissioned battery packs where the loading conditions vary between different stages of life and we deploy previously aged cells for a second life. To the best of our knowledge, no data set with such recommissioning data has been published yet.

Samsung INR18650-25R		
	Spec.	Unit
Chemistry	NCA	-
Max. voltage	4.2	V
Min. voltage	2.5	V
Max. cont. discharge current	20	A
Max. pulse current ($<$ 1 sec)	100	A
Rated capacity	2.5	Ah

Table 1. Li-ion battery cell specifications.

3. DESIGN OF EXPERIMENTS

3.1. Battery Type

We selected the INR18650-25R Li-ion battery cell manufactured by Samsung based on a Nickel-Cobalt-Aluminium chemistry (‘‘Introduction of INR18650-25R’’, 2013). A summary of the battery specifications provided by the manufacturer is listed in Table 1. We assembled two 18650 cells in series (2S) to replicate aging behavior of a pack instead of a single cell. We used double-layered nickel plates attached through spot welding to the electrode surfaces to accommodate the high current levels passing through the cells. To further improve the ability to handle high current levels we use 12 AWG copper wires in a double-wire electrode connection to split the current flow on the positive and negative side of the battery pack. A thermistor sensor at the ground connection of each pack allowed us to measure the cell surface temperature during cycling, Figure 1.

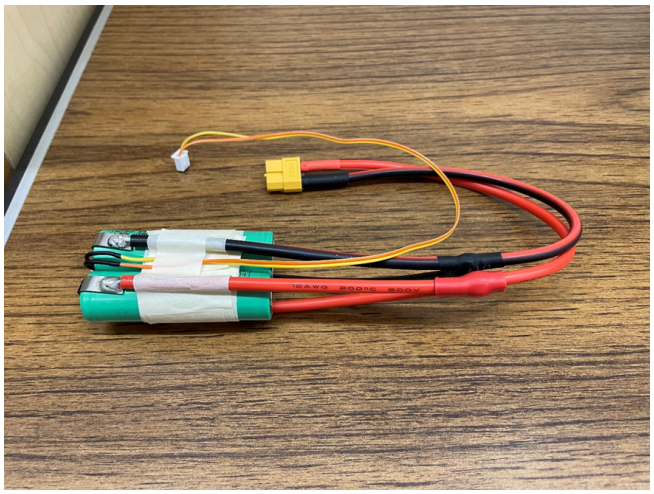

Figure 1. Fully assembled battery pack in 2S configuration.

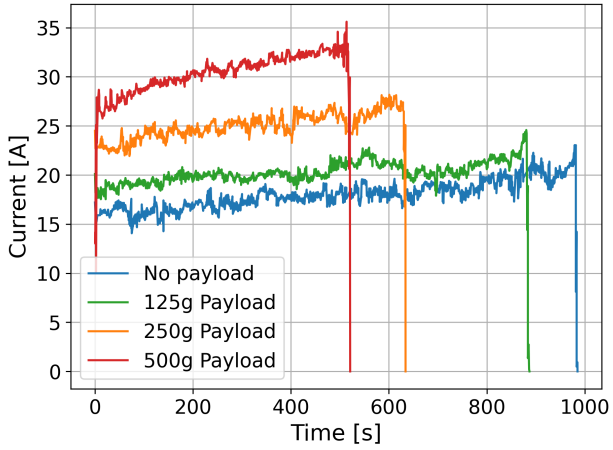

Figure 2. Load profile of a quadcopter drone during missions with different payloads.

3.2. Selection of Loading Profiles

This battery life cycle data set is intended to replicate battery aging resulting from operation similar to real-world applications. Possible real world deployments include the operations of quadcopters or eVTOLs. In case of small quadcopters, for example, waypoint-based missions might produce quasi-constant load while cruising in-between waypoints, and higher or lower current draw based on the relative direction between wind speed and trajectory, as well as within-mission changes of payload (e.g., package delivery). As an example of a load profile on a regular drone operation, Fig. 2 shows the current drawn from a battery deployed on a quadcopter drone subjected to different payloads. The signals refer to a steady-state condition where the drone hovered with different payloads, showing a quasi-constant current draw when the payload is fixed. These steady-state signals then changes during the different stages of flight, showing a step-wise behavior (ignoring short spikes due to maneuvers). Other battery powered applications like electric cars can also show large variations in loading conditions over the entire lifespan or within a single discharge cycle, e.g. aggressive discharge during longer uphill drives and mild battery loading during downhill drives.

Constant profile [A]				
9.3	12.9	14.3	16.0	19.0
Variable profile (avg. current) [A]				
14.3		17.0		

Table 2. Constant and variable current levels. Two batteries were subjected to each load level.

Therefore, we opted to design a life cycle experiment with batteries covering either constant or variable loading within the discharge cycles and mild as well as aggressive average loading over lifetime. Both constant and variable load levels expand over a wide range of possible battery discharge missions. To remain within the battery cell load limits of 20 A, we defined constant current levels ranging from 9.3A to 19.0A and variable load missions ranging from 13 to 16A and 16 to 19A. Table 2 lists the load levels for batteries that were subject to one loading condition. These load levels were assigned to two battery packs each.

Charging profiles and resting time were defined as follows: charging at 3 A constant current, with a rest phase of 10 minutes before each charge and discharge phases. This rest helped removing Li-ion concentration gradients within the cell. This choice allowed us to complete the experiments in a reasonable time while maintaining realistic load levels given the battery capacity.

Having in mind that battery packs can be subject to different loading conditions throughout their lives, e.g. more aggressive usage early in life and milder loading conditions later in life, we additionally opted to cycle battery packs subjected to different constant load levels at different stages of life. We selected 6 batteries that were cycled at two different load levels and two batteries subject to 3 different life cycle stages. Table 3 shows the load levels the recommissioned batteries were assigned to. For the first two load profiles (16 to 14.3 A, 14.3 to 16 A) we assigned 1 battery each, whereas two batteries each were cycled on the third and fourth profile (16 to 12.9 A, 16 to 9.3 A).

3.3. On the Estimate of Residual Capacity

As already mentioned in Section 4, the residual capacity of each battery was estimated using reference discharge cycles (very low and constant current level) at regular intervals. This mild loading discharge ensures small and negligible Li-ion concentration gradients between surface and bulk volumes of

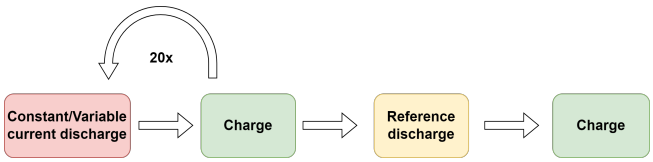

Figure 3. Life cycle operational procedure.

the two electrodes and prevents large temperature increases within the cell. Keeping Li-ion concentration gradients and temperature low is important for a correct estimation of battery capacity and ensures the reference discharge fulfills its sole purpose of estimating capacity opposed to further age the battery. Usually, a current level at or below the battery capacity (1 C) satisfies the requirements of the reference discharge cycle, which in case of the batteries used in this research, is equivalent to 2.5 A. We opted to perform the reference discharge cycle in regular intervals after 20 high current level discharges. Figure 3 shows the life cycle procedure used to age the battery packs.

3.4. Recommissioning of Used Cells

With the goal of producing a rich data set to investigate aging of battery packs, we reused battery cells from battery packs that were previously cycled until failure. Usually, within a failed battery pack, one cell experiences failure while the second cell is still functional. We removed the surviving cells from the 6 battery packs cycled at 16 A, 14.3 A and 12.9 A and reassembled them into 3 reusable packs. Those second-life battery packs were then deployed at less aggressive current levels compared to the loading conditions in their respective first lives. The goal of this life extension study is to see by how far reduced loading conditions can increase the life of already aged battery cells. Table 4 summarizes the load levels those reassembled battery packs were subject to during their first and second life.

3.5. Assessment of Cell Failure

To evaluate a battery pack failure, we measured the voltages across the positive and negative electrode of each cell. If at least one cell had a short circuit across the electrodes, due to internal damage or internal safety mechanisms that create an intentional short circuit to prevent a hazardous failure, we assumed the battery pack as failed. During each assessment, we checked that the short circuit was not created by disconnection of the nickel plate. We reinforced the welded contact in case we observed poor connection between plate and electrode, and re-measured voltage across the electrodes. Only in one instance, on battery pack 5.3, we observed a loose nickel plate connection after approximately 150 cycles. We fixed the contact between plate and electrode and the test proceeded normally afterwards.

3.6. Battery Numbering

We adopted a two-digit numbering, both starting from 0, that serves the purpose of identifying the battery packs, which slot they were tested on, and keeping track of the cells before and after the recommissioning testing. Battery X.Y means ‘‘testbed slot X, round Y,’’ where slot is the location on the testbed (0 to 5), and round refers to a single test, with each test corresponding to a battery pack. Therefore, round 0 correspond to the first battery pack tested on that slot, round 1 to the second battery pack tested on that slot, etc. For example, Battery 3.6 means that the data refers to the fourth slot of the testbed, and the 7th battery tested on that slot.

4. DATA SET OVERVIEW

In this Section, we present a summary of the data generated; from examples of voltage discharge time series to aging effects to outliers. The term ‘‘mission’’ utilized in this section means a full discharge profile, from fully charged to cutoff voltage.

4.1. Testing Summary

The cycling process ran continuously for 24 hours a day where 6 battery packs are aged simultaneously. The data set is organized in 3 different groups. The first contains data from batteries subject to a single loading profile. This can either be constant loading or variable loading conditions. The second group contains data from batteries subject to different loading types throughout their life; the loading cycles changed once or twice during testing. The third group contains data from second-life batteries, where cells from previous battery packs are combined into new packs and deployed at different current levels. A description of the data set organization and each data item can be found in Appendix A.

4.2. Discharge Time Series

A general overview of a 20 h excerpt of the data accumulated throughout a 24 h cycling process is presented in Fig. 4. The top plot shows voltage curves during discharge, and the bottom plot shows discharge currents. This cycle started with a reference discharge at 2.5 A for each of the six batteries, and is followed by discharges at higher current levels. This snapshot shows four batteries discharged at constant current levels (two at 16 A and two at 19 A), and two batteries discharged at variable current (between 16 A and 19 A).

Voltage time series are one of the most important data to characterize discharge and aging. Figure 5 shows an example of full discharge-charge cycle for each of the 6 batteries. The curves show: (i) a steep voltage drop during discharge, (ii) a 10 minute pause where regeneration effects are visible, (iii) a charge cycle at constant 3 A, and (iv) a 10-minute rest phase where the voltage plateaus due to ion concentration balancing between the bulk and surface volumes of each cell electrode.

Two life stages [A]				
Battery	(3.2)	(5.3)	(0.2, 3.3)	(1.2, 2.4)
First stage	16.0	14.3	16.0	16.0
Second stage	14.3	16.0	12.9	9.3
Three life stages [A]				
Battery		(0.3)	(2.5)	
First stage		16.0	16.0	
Second stage		14.3	7.5	
Third stage		7.5	14.3	

Table 3. Recommissioned batteries loading profiles.

Constant current [A] and Battery #			
First life	16.0 (0.0, 1.0)	14.3 (2.3, 5.2)	12.9 (3.1, 2.2)
Second life	9.3 (1.3)	7.5 (3.6)	5.0 (5.4)

Table 4. First and second life load profiles and corresponding batteries loads were applied to.

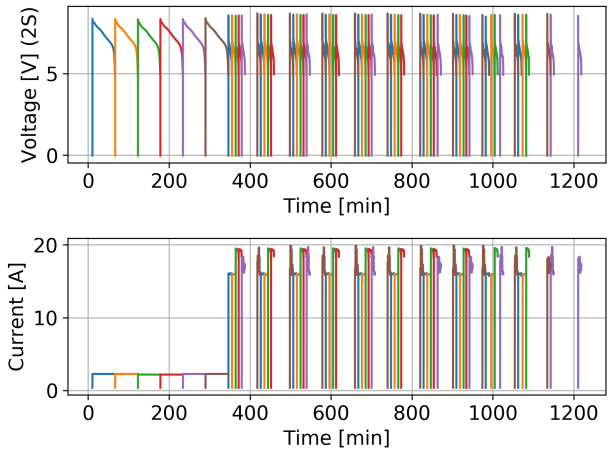

Figure 4. Snapshot of a day of test campaign, from the slow-discharge curves at the beginning of the test to the faster, high-current and random loading profiles. The six different colors refers to six different battery samples.

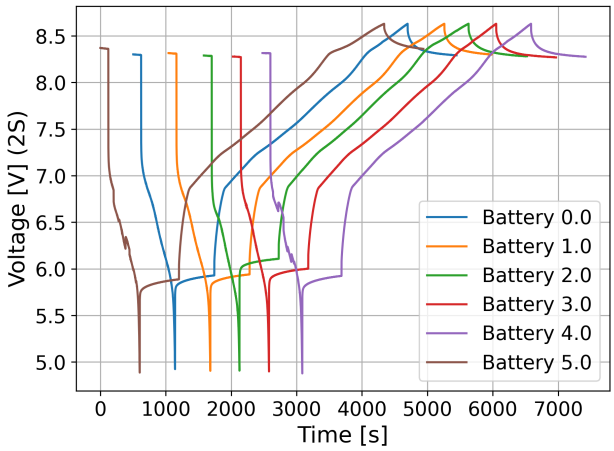

Figure 5. Voltage readings of an entire discharge and charge cycle for 6 batteries of the first battery batch. After a discharge cycle, the battery voltage recovers to roughly 6.0 V within the 10 minutes rest phase.

The next discharge cycle then begins.

4.3. Loading Profiles

Figure 6 shows current, voltage and temperature readings within one early-life discharge at constant current and variable current. The variable-current mission is designed as step-wise constant, with prescribed switching to different current levels every 40, 60 or 80 seconds, selected randomly with equal probability. The current levels were also selected randomly within the defined upper and lower bounds for the different missions. A pre-defined set of mission profile was generated off-line and then applied throughout the 24h cycling process. When using constant-current profiles, a minor current drop happens shortly before reaching EOD. The starting point is not equal to the fully charged voltage of 8.4V due to the instantaneous application of high discharge current levels above 4 C that cause a large initial voltage drop. The rapid change of voltage at the corresponding current steps is an expected behavior following Ohm's law. The temperature readings for this example, measured on the surface of one cell electrode, starts at room temperature and reaches maximum temperatures of 105 °C and 95 °C in the constant and variable load case, respectively.

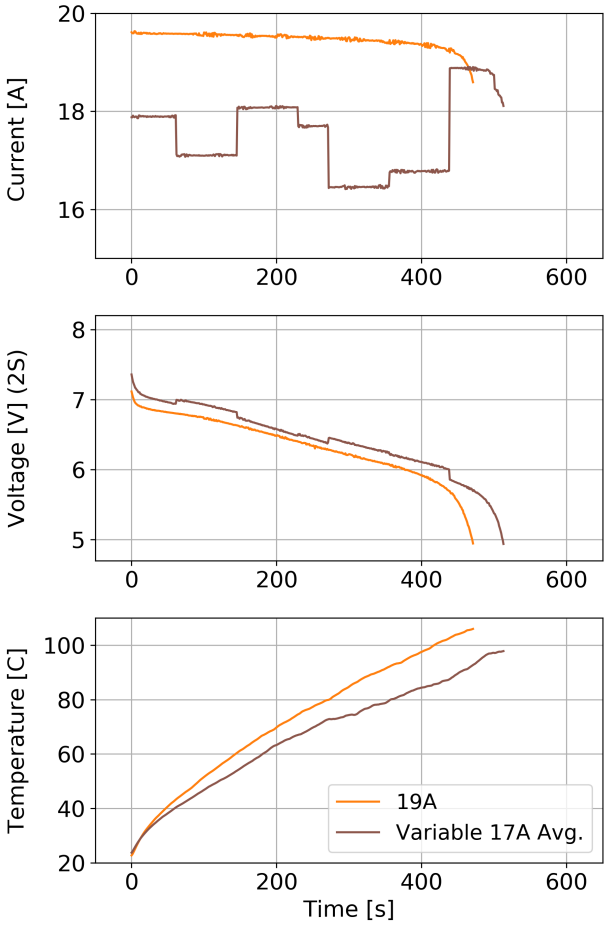

Figure 6. Current, voltage and temperature readings for two batteries discharged at constant and variable load.

4.4. Aging Effect and End-Of-Life

The life cycling process was continued until reaching EOL, which was defined as the occurrence of cell failure in at least one cell of the battery pack. Cell failure typically corresponded to a short circuit between the positive and negative cell electrode (see Section 3.5). Figure 7 shows an example of the phenomenological effect aging has on voltage curves at constant and variable loading discharge cycles. According to our nomenclature, ‘‘Mission’’ in the legend refers to the number of discharge cycles the battery was subject to. Here, all loading conditions remain either identical (in the case of constant-loading profile) or statistically the same (in the case of variable-loading profiles) throughout the tests. The shorter time to discharge as well as the lower intercept of the linear portion are purely due to battery aging.

As one of the main goal of the life cycle testing is to characterize the battery capacity degradation over time, we provide an example of minimally post-processed data: the residual capacity C as a function of the cumulative energy draw E.

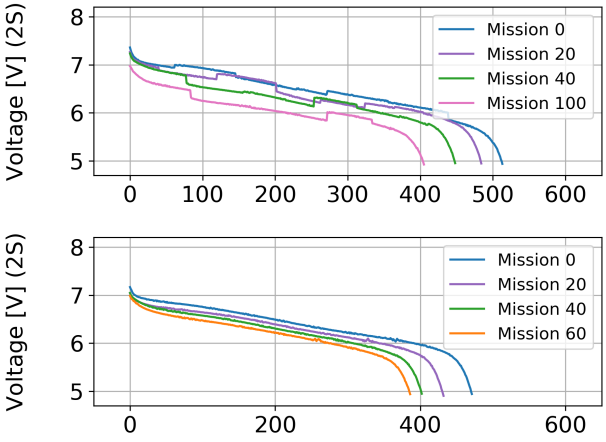

Figure 7. Variable current (16 - 19 A, top panel) and constant current (19 A, bottom panel) discharge missions at different life stages.

Capacity degradation as function of cumulative energy can serve as a surrogate to battery life time. To obtain such a curve, first we need to obtain capacity C as the integral of current draw over time t:

$$C = \int_0^t A_\tau \, \mathrm{d}\tau \approx \sum_k A_{t_k} \cdot \Delta t_k \ ,$$

where A_{t_k} is the current value at time t_k and Δt_k represents the time delta between the current and previous time step. Similarly, cumulative energy E at time t can be expressed as:

$$E = \int_0^t A_\tau \cdot V_\tau \, \mathrm{d}\tau \approx \sum_k A_{t_k} \cdot V_{t_k} \cdot \Delta t_k \ ,$$

where V_{t_k} is the voltage at time t_k. Figure 8 shows capacity degradation curves for constant and variable load cases; for clarity, only batteries subject to one loading condition are shown. As mentioned earlier, two battery packs were assigned to each load level. Each data point represents the capacity from one reference discharge, whereas failures are marked by **x**. For reference, the capacity degradation curve from the manufacturer's datasheet for 20 A is plotted as a gray line. We can see a wide spread of the capacity degradation curves and corresponding EOL caused by the large range of load levels.

4.5. Outliers

In this sub-section we want to address data outliers and abnormalities detected thus far during post-processing and data analysis.

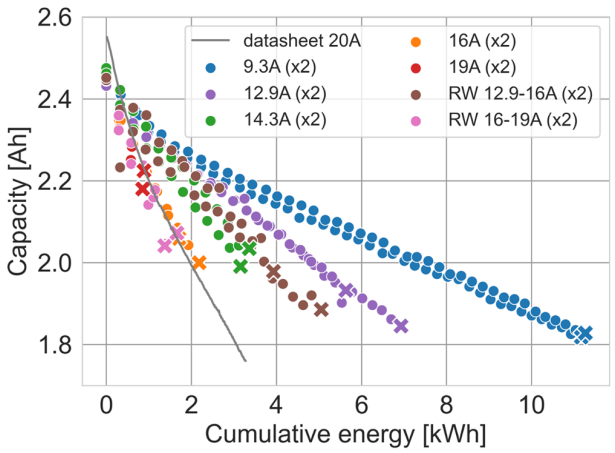

Figure 8. Capacity degradation over cumulative energy for batteries subjected to constant and variable loading. Cell failures are marked by **x**.

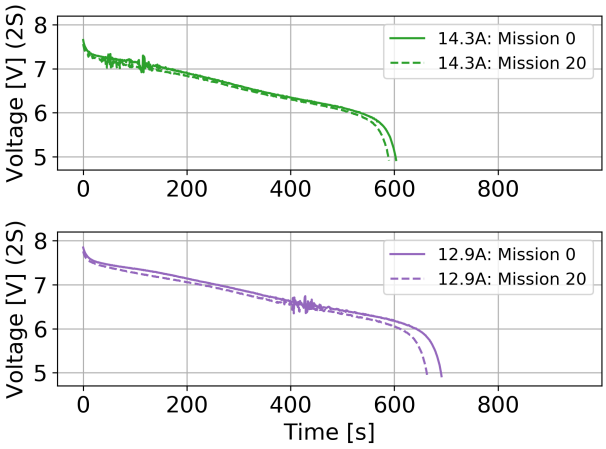

Figure 10. Noise in voltage sensor reading.

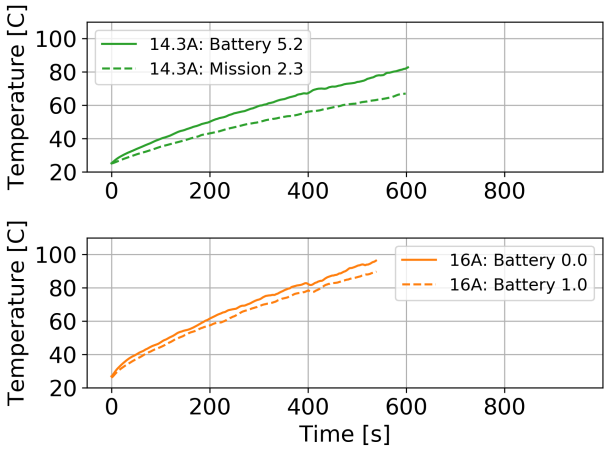

Figure 9. Temperature build-up within first mission of batteries subjected to 14.3A and 16A loading.

4.5.1. Temperature Readings

Generally, temperature readings from batteries subject to the same load profile is fairly close to one another, but due to the manual placement of the thermistor sensor to the nickel plate connection using thermal glue, on top of natural variability due to manufacturing processes, inter-specimen (i.e., battery-to-battery) variations naturally occurred. In case of 14.3 A constant-current discharge (Batteries 2.3 and 5.2) the observed difference is significant. The result is reported in Fig. 9, top panel. The temperature reaches around 80 °C for battery 5.2 but only around 65 °C for battery 2.3. For reference to a ‘‘standard’’ case, the bottom panel of Fig. 9 shows the 16 A load applied to Batteries 0.0 and 1.0, which maximum temperature was recorded as 98 °C and 93 °C, respectively.

In rare instances, the batteries placed on charger slot 2 logged an invalid temperature reading due to thermistor connection issues.

4.5.2. Sensor Noise

The data acquisition is based on analog-digital converter (ADC) chips, which read analog voltage, current and temperature sensor values. Voltage readings rely on a voltage divider to keep values within bounds of the ADC. In some instances, noisy behavior was visible in the signals, as shown in Figure 10. When sensor noise was first observed, it was repeatedly detected at the same voltage level and load amplitude. As the observed phenomenon had no impact on the testing procedure and minor impact on the main test results, we did not pursue further investigation into its underlying causes.

4.5.3. Cycle Interruptions Due to Relay Malfunctions

The charger path relay occasionally failed to open the connection between battery and charger module due to a coil malfunction. Figure 11 presents the voltage curves measured on the charger board for a ‘‘regular’’ and a relay-malfunction cycle. In both cycles the charger relay is activated but, due to the relay malfunction, in one case the battery remains at rest.

This happened rarely, when a battery completed its resting phase after discharge and the microcontroller provided the digital signal for the charger module to the battery connection, but the analog voltage operating the relay coil was not sufficient to open the relay path. In this scenario, the battery remained in resting state and a restart of the entire testbed was necessary. If another battery happened to be within a discharge cycle, the manual restart was postponed until after the discharge cycle was finished to ensure that every discharge was completed.

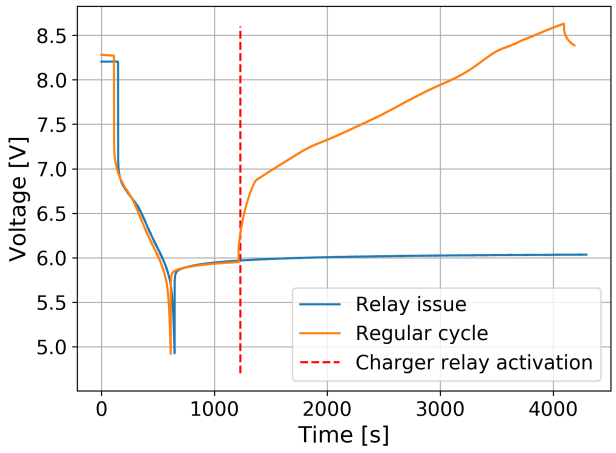

Figure 11. Charger relay malfunction effect on voltage.

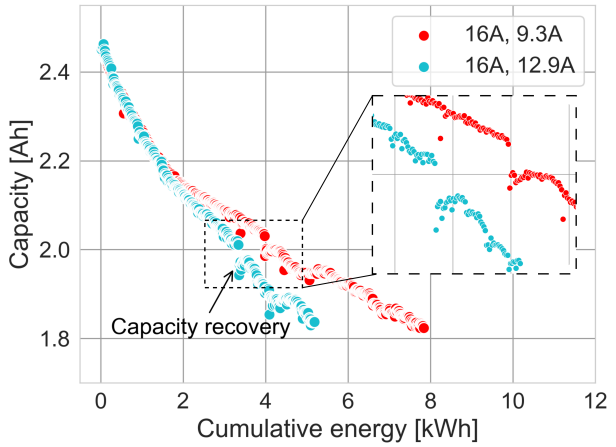

Figure 12. Capacity recovery after cycling pause.

4.6. Other Factors

During testing of 4 batteries subject to two load levels, an interruption of the cycling process for approximately 30 days became necessary. The batteries that have been affected are: Battery 2.4 and 0.2 (loaded with 16 A first, 9.3 A later), and Batteries 1.2 and 3.3 (loaded with 16 A first, 12.9 A later). After restarting the life cycle process, we observed slightly different capacity values, which normalized after a few days of continued cycling. Figure 12 shows the initial drop of capacity after a cycling pause of 4 weeks and the slight capacity recovery within the first few life cycles.

Furthermore, due to a centralized temperature control of the ambient air temperature in the testing laboratories, a temporary temperature drop caused a reduced battery capacity which recovered right after the return to the regular air temperature of approximately 23°C. This temperature abnormality affected battery packs 0.2, 2.4, 1.2 and 3.3 within a range of 3 to 5 kWh of battery pack age.

5. TESTBED DESIGN AND DEVELOPMENT

The testbed is designed to continuously cycle up to 6 batteries at different discharge load levels and constant current charging, Fig. 13. It is built on a vertical rack that includes a bottom level where the motherboard, based on a printed circuit board (PCB), microcontroller and AC-DC converter for the general 12V supply of the system is placed. Six identical charger board levels follow above, each accommodating a charger PCB including a DC-DC step-down converter, a 12V AC-DC converter as power supply for charging, as well as a slot for one battery pack. The top level of the test-rig is reserved for the load PCB, which includes active cooling systems, and is designed to function as discharge board to create a load for controlled discharge.

Figure 14 shows all 3 different types of boards that were designed using an online PCB design tool, printed and, after assembly, integrated in the testbed. The picture on the left-hand side shows the motherboard used as control system for the entire testbed, where we integrated the Arduino Nano Every microcontroller. A SD card breakout board hosting a microSD card is also embedded in the motherboard, and is used for data-logging and storage of test metadata that is read and executed by the microcontroller. To ensure safe and reliable communication between the microcontroller and the remaining components we use the I2C communication protocol, where a I2C multiplexer is used to split the signals in different buses, which became necessary to establish communication with the identical I2C components on the 6 charger boards. We also equipped the motherboard with a WiFi module for wireless access to the data readings during the cycling process.

The board depicted in the center of Figure 14 serves as the charger board. Its primary function is to charge the connected battery using a DC-DC step-down converter. Additionally, it controls the pathway, allowing for connection to either the charger module or the load board. We integrated the XL4015 DC-DC step down converter to charge batteries at controlled current levels, with a maximum charge current of 4 A. The XL4015 is provided with 12V DC voltage from a separate 12V AC-DC converter. The board integrates two high-power rated relays with continuous current ratings up to 35A that control the path between the connected battery to either the charger module or load board. For both the battery connection and load path we use a 12AWG wire that is connected via solder pads to the charger board. A XH-connector is used for the I2C communication wire and the battery cell temperature sensor connection. The PCB design integrates digital-analog-converter (DAC) and ADC microchips for signal conversion to and from the I2C bus, used for relay operation and data acquisition from the voltage, current and temperature sensors.

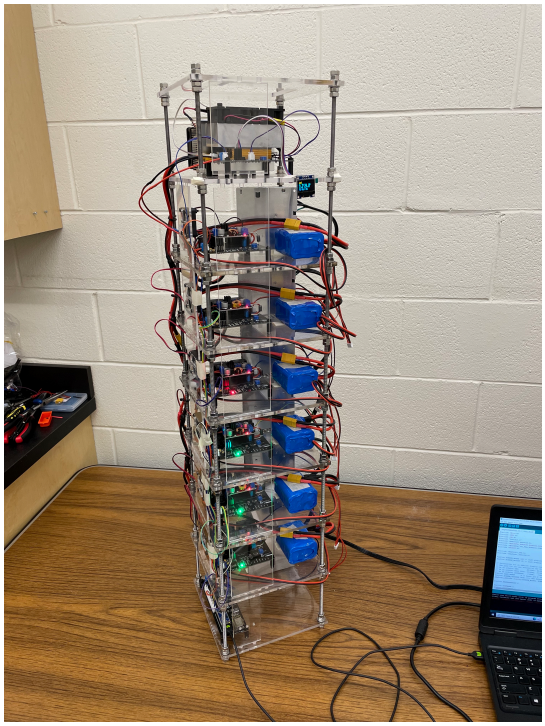

Figure 13. Testbed in operation.

The rightmost PCB represents the load board on Figure 14, which is used to discharge the batteries at the desired current levels. The board uses 4 IRF250 high power rated N-channel MOSFETs to control the current levels, where an operational amplifier (Op-amp) is used to drive the MOSFET gates through a feedback control circuit. The Op-amp in turn receives its analog target value from a DAC that is controlled through the microcontroller with digital control signals. Due to the high levels of power dissipation handled through the MOSFETs, a heatsink with active cooling is placed in direct surface connection to the MOSFETs to control the temperature buildup. In order to measure the actual discharge current, we opted to integrate two 100 W rated current sense resistors with a resistance of 0.1 Ω, where the voltage drop across the resistors is measured and converted to digital signals through an ADC, which is then used to estimate the current flow. The board also measures the temperature on the power MOSFETs as well as the current sense resistors to ensure operation within safety limits. A loadbus connection establishes a path from the load board to all 6 charger boards via a shared 12AWG bus cable.

5.1. Controls and Functionality

Figure 15 gives an overview over the functionality and dependencies of each submodule integrated in the testbed. As previously mentioned a 12V DC power supply provides all boards with a basic operating voltage used for the microchips. The I2C communication is established from the motherboard to each charger board and the load board. Each charger board is equipped with a separate 12V supply for battery charging and is connected to one battery each. And a shared load bus is used to connect the batteries via the charger boards to the load board.

The microcontroller acts as the brain of the entire system while functioning as a statemachine. The controller code is written in C++, where the main task is the mission scheduling following a predefined mission plan with discharge missions and charge phases, taking into account resting time between charge phases and missions. The microcontroller converts mission information from the mission plan into specific discharge current target setpoints forwarded to the load board and logs the acquired data readings. Additionally, safety mechanisms for operational safety are implemented in the controller code, which ensure operational shutdown if temperature, current and voltage limits are violated. The code operates through a single iteration over a setup function, which establishes the I2C communication to all components, initializes operational parameters through reading global variables from the SD card and initializes the battery and mission structures which contain both the planned mission information and stores data readings before logging. After the setup, a continuous loop function reads the the previous states, controls the batteries and logs the updated battery states on the microSD card as well as prints the state on a serial monitor. The iteration over the main loop and the data logging is executed with a frequency of 1Hz.

ACKNOWLEDGMENT

The work of Matteo Corbetta and Chetan Kulkarni was supported by the System-Wide Safety (SWS) project under the Airspace Operations and Safety Program within the NASA Aeronautics Research Mission Directorate (ARMD). The authors want to thank the NASA Ames Prognostics Center of Excellence for hosting the data set in its public data repository.

REFERENCES

Attia, P., Grover, A., Jin, N., Severson, K., Markov, T., Liao, Y.-H., ... Chueh, W. (2020, 02). Closed-loop optimization of fast-charging protocols for batteries with machine learning. *Nature*, *578*, 397-402. doi: 10.1038/s41586-020-1994-5

Bole, B., Kulkarni, C., & Daigle, M. (2014). *Randomized battery usage data set.* NASA Ames Research Center, Retrieved 11 May 2020. Moffett Field, CA: NASA Ames Research Center. Retrieved from `http://ti.arc.nasa.gov/project/prognostic-data-repository`

Girishkumar, G., McCloskey, B., Luntz, A. C., Swanson, S., & Wilcke, W. (2010). Lithium-air battery: promise and challenges. *The Journal of Physical Chemistry Letters*, *1*(14), 2193--2203.

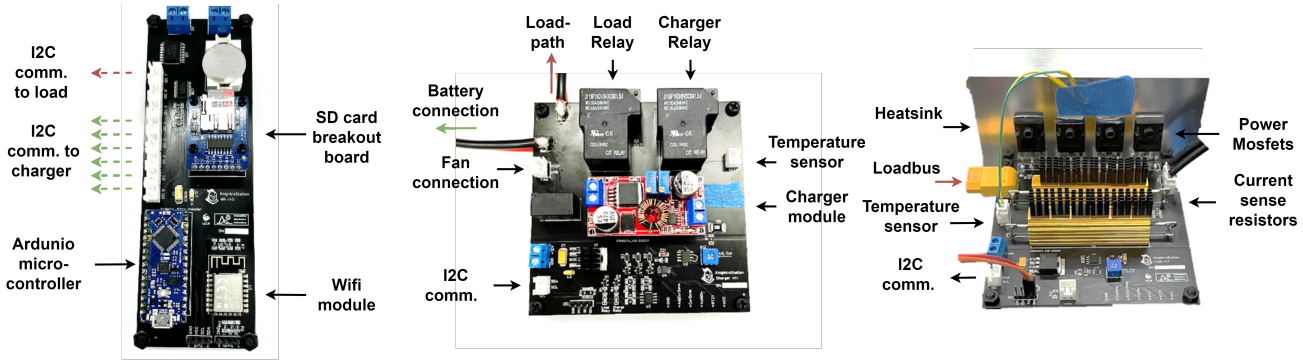

Figure 14. Printed circuit boards: motherboard (left), charger board (middle), and load board (right).

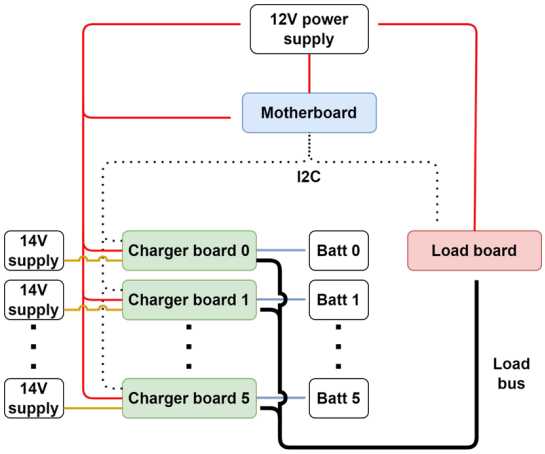

Figure 15. Testbed functionality schematics.

Govindarajan, J. (2021). *Lifecycle ageing tests on commercial 18650 li ion cell @ 10°c and 0°c.* 4TU.ResearchData. Retrieved from https://data.4tu.nl/articles/dataset/Lifecycle_ageing_tests_on_commercial_18650_Li_ion_cell_10_C_and_0_C/14377295/1 doi: 10.4121/14377295.V1

He, W., Williard, N., Osterman, M., & Pecht, M. (2011, 12). Prognostics of lithium-ion batteries based on dempster–shafer theory and the bayesian monte carlo method. *Journal of Power Sources*, *196*, 10314-10321. doi: 10.1016/j.jpowsour.2011.08.040

Hwang, J.-Y., Myung, S.-T., & Sun, Y.-K. (2017). Sodium-ion batteries: present and future. *Chemical Society Reviews*, *46*(12), 3529--3614.

Introduction of inr18650-25r [Computer software manual]. (2013, 10).

Karthikeyan, D. K., Sikha, G., & White, R. E. (2008). Thermodynamic model development for lithium intercalation electrodes. *Journal of Power Sources*, *185*(2), 1398--1407.

Li, S., He, H., Su, C., & Zhao, P. (2020). Data driven battery modeling and management method with aging phenomenon considered. *Applied Energy*, *275*, 115340.

Lutsey, N., & Nicholas, M. (2019). Update on electric vehicle costs in the united states through 2030. *Int. Counc. Clean Transp*, *12*.

Preger, Y., Barkholtz, H., Fresquez, A., Campbell, D., Juba, B., Romàn-Kustas, J., ... Chalamala, B. (2020, 08). Degradation of commercial lithium-ion cells as a function of chemistry and cycling conditions. *Journal of the Electrochemical Society*, *167*. doi: 10.1149/1945-7111/abae37

Raj, T. (2020). Path dependent battery degradation dataset part 1.

Raj, T., Wang, A. A., Monroe, C. W., & Howey, D. A. (2020). Investigation of path-dependent degradation in lithium-ion batteries. *Batteries & Supercaps*, *3*(12), 1377--1385.

Saha, B., & Goebel, K. (2007). *Battery data set.* NASA Ames Research Center, Retrieved 11 May 2020. Moffett Field, CA: NASA Ames Research Center. Retrieved from http://ti.arc.nasa.gov/project/prognostic-data-repository

Severson, K., Attia, P., Jin, N., Perkins, N., Jiang, B., Yang, Z., ... Braatz, R. (2019, 05). Data-driven prediction of battery cycle life before capacity degradation. *Nature Energy*, *4*, 1-9. doi: 10.1038/s41560-019-0356-8

Shen, S., Sadoughi, M., Li, M., Wang, Z., & Hu, C. (2020). Deep convolutional neural networks with ensemble learning and transfer learning for capacity estimation of lithium-ion batteries. *Applied Energy*, *260*, 114296.

Trad, K. (2020). D2. 3-report containing aging test profiles and test results. In *Tech. rep.* EVERLASTING.

Trad, K. (2021). *Lifecycle ageing tests on commercial 18650 li ion cell @ 25°c and 45°c.* 4TU.ResearchData. Retrieved from https://data.4tu.nl/articles/_/13739296/1 doi: 10.4121/13739296.V1

Williard, N., He, W., Osterman, M., & Pecht, M. (2013, 03). Comparative analysis of features for determining state of health in lithium-ion batteries. *International Journal of Prognostics and Health Management*, *4*. doi:

10.36001/ijphm.2013.v4i1.1437

Xing, Y., Ma, E., Tsui, K.-L., & Pecht, M. (2013, 06). An ensemble model for predicting the remaining useful performance of lithium-ion batteries. *Microelectronics Reliability*, *53*, 811–820. doi: 10.1016/j.microrel.2012.12.003

Yabuuchi, N., Kubota, K., Dahbi, M., & Komaba, S. (2014). Research development on sodium-ion batteries. *Chemical reviews*, *114*(23), 11636--11682.

A. DATA SET REPOSITORY STRUCTURE

The data set repository is organized into three main folders, each containing one group of life cycled battery packs.

A.1. Folders

These are the sub-folders in the data set:

- Regular accelerated life test (‘‘regular_alt_batteries’’ folder):
  This folder contains the data files from battery packs subject to constant and variable loading conditions, where the current range of the latter remains the same throughout the battery life. The assigned battery packs in this folder are numbered as follows:
  - Constant current:
    - 9.30 A: Battery pack 0.1 and 1.1
    - 12.9 A: Battery pack 3.1 and 2.2
    - 14.3 A: Battery pack 2.3 and 5.2
    - 16.0 A: Battery pack 0.0 and 1.0
    - 19.0 A: Battery pack 2.0, 3.0 and 2.1
  - Variable current:
    - 14.3 A (mean current): Battery pack 4.1 and 5.1
    - 17.0 A (mean current): Battery pack 4.0 and 5.0
- Recommissioned batteries (‘‘recommissioned_batteries’’ folder):
  This folder contains the data files from battery packs where the constant loading conditions were changed throughout the battery life. The assigned battery packs in this folder are numbered as follows:
  - Two life stages:
    - 16 A, 14.3 A: Battery pack 3.2
    - 14.3 A, 16 A: Battery pack 5.3
    - 16 A, 12.9 A: Battery pack 0.2 and 3.3
    - 16 A, 9.30 A: Battery pack 1.2 and 2.4
  - Three life stages:
    - 16 A, 14.3 A, 7.5 A: Battery pack 0.3
    - 16 A, 7.5 A, 14.3 A: Battery pack 2.5
- Second life batteries (‘‘second_life_batteries’’ folder):
  This folder contains the data files from battery packs that consist of battery cells which survived cycling as part of previously cycled battery packs. The assigned battery packs in this folder are numbered as follows:
  - Second life battery packs:
    - 16.0 A, 9.3 A: Battery pack 1.3
    - 14.3 A, 7.5 A: Battery pack 3.6
    - 12.9 A, 5.0 A: Battery pack 5.4

A.2. Files

Within each folder, individual battery packs own their dedicated csv file for continuous data logging, which are named with their respective battery pack number. The columns in each csv file contain the following data: ‘‘start time’’, ‘‘relative time’’, ‘‘mode’’, ‘‘voltage charger’’, ‘‘temperature battery’’, ‘‘voltage load’’, ‘‘current load’’, ‘‘temperature mosfet’’, ‘‘temperature resistor’’, ‘‘mission type’’.

The first column provides the date and time in form:

[mm:dd:yyyy hh:mm:ss]

for each of the 24h cycling missions. The second column contains the relative time [s] from the start of the entire cycling process for each battery pack. The third column provides information about the mode, where the digits -1, 0, 1 represent discharge, rest and charge in respective order. Column 4 provides the continuous battery pack voltage [V] measured on the charger board. Column 5 provides the battery pack temperature reading [°C] throughout the entire process. Columns 6 and 7 contain the voltage [V] and current [A] readings measured on the load board during discharge, and columns 8 and 9 provide the temperature readings from the MOSFETs [°C] and current sense resistor [°C] on the load board. Column 10 contains the mission type information, which is defined as either 1 for a regular discharge mission or 0 if a reference discharge is performed.